TW2-TTMS-001b-D02

Task Title: IRRADIATION PERFORMANCE NEUTRON IRRADIATION TO 70 dpa AT 325°C AND PIE

INTRODUCTION

The main objective of this experiment is to study the irradiation behaviour of Reduced Activation Ferritic/Martensitic (RAFM) steels, in particular the European reference Eurofer 97, at high doses and for irradiation temperatures lower than 400°C, where materials are susceptible to reach a high level of hardening and embrittlement.

For this purpose, irradiations experiments were conducted in the BOR60 reactor of the Research Institute of Atomic Reactors (RIAR, Dimitrovgrad, Russia) at 325°C.

This task includes two items:

a) The Post Irradiation Examinations (PIE) corresponding to specimens irradiated up to 42 dpa in "ALTAIR" experiment (1st phase) that finished in 2002.

b) A 2nd phase of irradiation named "ARBOR 2" (FZK-CEA joint experiment) performed in the same reactor for 40 dpa at the same temperature.

2005 ACTIVITIES

Specimens included in ALTAIR irradiation experiment have reached a dose ranging from 32 dpa up to 42 dpa. The corresponding PIE was conducted in the hot cells of RIAR. The profilometry of pressurized tubes, to determine the irradiation creep modulus, was presented in the Annual Report of the Association EURATOM-CEA 2004. Tensile and Charpy tests as well as fractographic examinations were completed in the first half 2005.

On the other hand, ARBOR 2 experiment, started in january 2003 and finished on may 2005 according to the initial schedule. The doses reached ranged from 30 to 41 dpa, giving a total dose of 65-80 dpa in samples previously irradiated in ALTAIR experiment.

PIE OF SPECIMENS IRRADIATED IN ALTAIR EXPERIMENT

The irradiation in the BOR60 reactor was performed at 325±5°C for doses ranging from 32.5 to 42.3 dpa. The following materials were irradiated as specimens for mechanical tests: RAFM steels EUROFER (9Cr-1W-0.18V-0.15Ta) and 9Cr2WTaV (9Cr-2W-0.24V-0.08Ta), the advanced alloy ODS-MA957 (Fe-14Cr-1Ti-0.3Mo-0.25Y_2O_3), and conventional martensitic steels, 9Cr-1Mo and 9Cr-1MoVNb. Tensile tests were performed at 20 and 325°C using a strain-rate of $1.4x10^{-3}.s^{-1}$ on specimens of 2 mm diameter and 12 mm gauge length. Impact properties were determined with Charpy-V subsize specimens of 3x4x27 mm^3 with T-L orientation. Details are given in ref. [1], [2].

TENSILE TESTS

Irradiated specimens were tested at 20°C and at the irradiation temperature (325°C). Tests were also performed on control (unirradiated) samples for comparison.
The tensile curves of RAFM steels and ODS alloys are compared to those of commercial martensitic steels, standard 9Cr1Mo (EM10) and modified 9Cr1MoVNb (T91), irradiated in the same conditions as shown in figure 1.

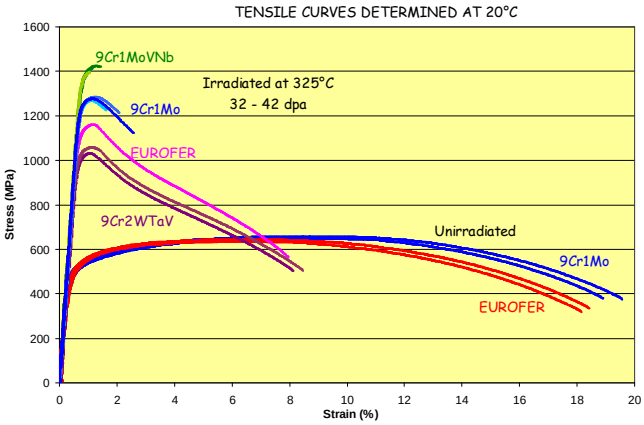

Figure 1: Stress-strain curves of 9Cr-martensitic steels irradiated up to 42 dpa at 325°C in BOR60 reactor compared to the unirradiated condition

All materials display irradiation-induced hardening, determined by the increase of the yield stress, but the magnitude depends on the material. The increase of tensile strength is associated to a reduction of the ductility also depending on the material.
The highest hardening-level at 40-42 dpa was reached for 9Cr1MoVNb and 9Cr1Mo conventional steels, whereas RAFM-steels, EUROFER and 9Cr2WTaV, exhibited lower hardening. These 9%Cr-martensitic materials presented quite similar tensile properties before irradiation, but they evolved in a different manner during irradiation.

The comparison of data from BOR60 and irradiation experiments performed in OSIRIS (CEA) and SM2 (RIAR) reactors allows evaluating the effects of dose on the evolution of the tensile properties up to 42 dpa.
The dose dependence of irradiation-induced hardening, measured by the increase of the yield-stress, is shown in figure 2. A very rapid increase of hardening is observed for all materials up to about 10 dpa with a continuous decrease of the hardening-rate; beyond this value there could be a tendency to saturation in the case of 9Cr1Mo steel. Data obtained at high dose (32.5-42.3 dpa) for EUROFER and

9Cr2WTaV seem to follow the same trend of F82H and JLF-1 at low dose (<15 dpa). Therefore, the behaviour of all RAFM steels is represented by a unique curve.

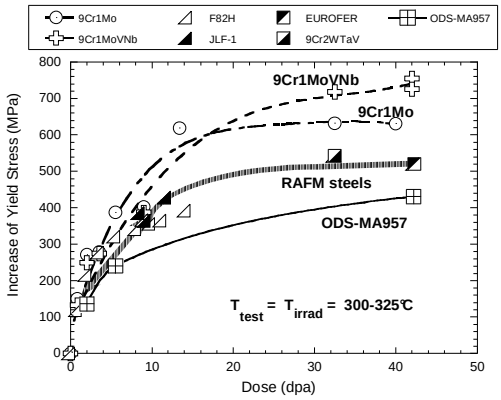

Figure 2: Evolution of the irradiation-induced hardening at 300-325°C, measured by the increase of the yield stress, as a function of the dose. Data obtained from experiments performed in OSIRIS (1 - 9 dpa), SM2 (8 – 14 dpa) and BOR60 (32 – 42 dpa) reactors.

The increase of tensile strength is associated with a ductility drop given by the decrease of total and uniform elongation as well as the reduction-in-area values. As shown in figure 3, the total elongation of RAFM steels for low doses decreases much faster than that of the 9Cr1Mo standard. Above 15 dpa the ductility loss of RAFM steels seems to be stabilized whereas the total elongation of 9Cr1Mo continues to decrease to reach very poor values (<2%), especially for tests performed at 20°C. However, a nearly saturated hardening is detected for 9Cr1Mo by 10 dpa. Regarding the uniform elongation, very low levels in the range 0.3-0.5% were obtained at both test temperatures for RAFM and 9Cr1MoVNb steels since 2 dpa, but 9Cr1Mo preserves higher values of uniform elongation up to 10 dpa.
It is worthwhile to notice the interesting behaviour of the ODS-Fe14%Cr ferritic alloy. This material exhibited the lowest hardening (430 MPa) and the highest values of total and uniform elongation at 42 dpa confirming the trend previously observed at lower doses in OSIRIS experiments.

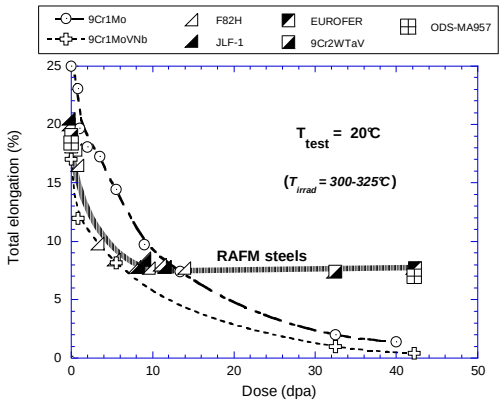

Figure 3: Dependence of the total elongation with the dose. Data, obtained at room temperature, from experiments performed in OSIRIS (1 - 9 dpa), SM2 (8 – 14 dpa) and BOR60 (32 – 42 dpa) reactors.

IMPACT PROPERTIES OF 9Cr MARTENSITIC STEELS

The irradiation-effects on impact properties were investigated on EUROFER, 9Cr2WTaV and 9Cr1Mo irradiated in BOR60. Energy transition curves, determined from Charpy tests, are shown in figure 4 for irradiated and unirradiated conditions. Before irradiation, the Ductile-Brittle Transition Temperature (DBTT) was about -100°C/-80°C for these materials.
After irradiation at 325°C, an important degradation of impact properties, i.e., an increase of the DBTT associated with a significant decrease of the Upper Shelf Energy (USE) values, is observed for all materials. The DBTT-shift is about 150°C for 9Cr2WTaV (32.5dpa), 200°C for EUROFER (42 dpa), about 250°C for 9Cr1Mo (40 dpa). The last material also exhibits a huge degradation of the USE. Similar behaviour was found for 9Cr1MoVNb steel.
RAFM steels present a lower degree of irradiation-induced embrittlement compared to 9Cr1Mo-type conventional steels in agreement with the behaviour of tensile properties.

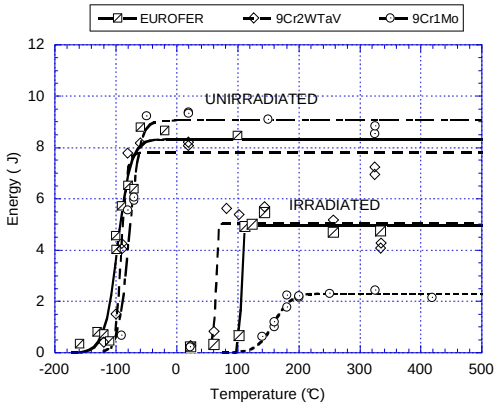

Figure 4: Comparison of impact properties of EUROFER, 9Cr2WTaV and 9Cr1Mo steels in the unirradiated condition and after irradiation in BOR60 reactor at 325°C for 32-42 dpa.

On the other hand, the present results illustrate the important effect of irradiation-temperature on the irradiation behaviour of materials. Figure 5 shows the dependence of DBTT values with the irradiation temperature determined for different ferritic-martensitic steels from experiments performed in PHENIX reactor at high doses (70-100 dpa). In particular, 9Cr1Mo-(EM10) conventional steel exhibited very stable mechanical properties in the range 380-550°C, where the DBTT values were lower than room temperature after irradiation. This behaviour is in contrast with that observed below 380°C, where the magnitude of hardening and embrittlement strongly increases with the decreasing irradiation temperature.
Consequently, these results put forward the dominant effect of the irradiation-temperature on materials behaviour and show the important degree of induced-hardening and embrittlement that could be expected for temperatures lower than 400°C. This fact is an important concern for applications of 9Cr-martensitic steels in this range of temperatures.

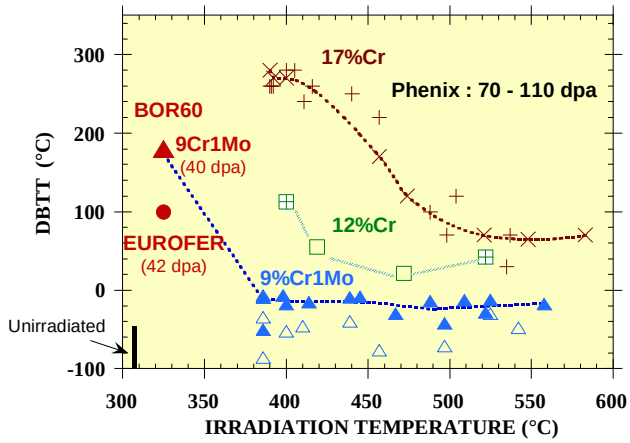

Figure 5: Dependence of DBTT values with the irradiation temperature. Comparison of data obtained from Phenix experiments (J.L. Séran et al. , JNM 212-215 (1994) 588) and the present work.

CONCLUSIONS

The irradiation behaviour of EUROFER-9Cr1WTaV, other RAFM martensitic steels, 9Cr1Mo conventional steels and ODS-Fe-14%Cr was studied after neutron irradiations performed at 325°C in BOR60 fast-reactor for high doses (32-42 dpa). The main conclusions are:

- Significant irradiation-induced hardening was obtained for all materials after irradiation at 325°C up to 42 dpa, the highest level was reached for 9Cr1Mo-type steels.

- At high dose, EUROFER and 9Cr2WTaV RAFM-steels preserved a significant total elongation level. But, a continuous ductility loss with the dose was observed for 9Cr1Mo steels.

- Irradiation at 32-42 dpa induced a very important DBTT-shift for all materials, 150-200°C for RAFM steels, 250°C for 9Cr1Mo alloys, associated with a decrease of USE-level.

- In general, a better behavior was found for RAFM-9CrWTaV martensitic steels, which displayed lower level of hardening and embrittlement compared to conventional steels.

- EUROFER, 9Cr2WTaV and 9Cr1Mo martensitic steels presented a very low irradiation-creep deformation (less than 1%) after irradiation for 63 dpa at 325°C.

- For temperatures lower than 400°C, the hardening and embrittlement of 9Cr-steels are strongly determined by the irradiation-temperature. However, their magnitude seems to depend also on the chemistry and the metallurgical condition of steels.

- In spite of its high-Cr content, ODS-Fe14%Cr presented the lowest hardening-level and high residual ductility after irradiation at 42 dpa.

REPORTS AND PUBLICATIONS

[1] A. Alamo, P. Wident, V. Shamardin, "Post-irradiation examinations of materials irradiated in BOR 60 reactor at 325°C up to 42 dpa. Final Report TW2-TTMS-001b-D02, CEA report DMN/SRMA/N.T. SRMA 2006-, march 2006.

[2] A. Alamo, J.L. Bertin, P. Wident, V. Shamardin, "Mechanical properties of 9Cr martensitic steels and ODS-FeCr alloys after neutron irradiation at 325°C up to 42 dpa", oral communication ICFRM-12, Santa Barbara, US, Dec.4-9 2005, to be published in J. of Nuclear Materials.

TASK LEADER

Ana ALAMO

DEN/DMN/SRMA
CEA-Saclay
F-91191 Gif sur Yvette Cedex

Tel. : 33 1 69 08 67 26
Fax : 33 1 69 08 71 67

e-mail : ana.alamo@cea.fr

Not available on line

Not available on line

Not available on line

Not available on line

Not available on line

Not available on line

Not available on line

Not available on line

TW4-TTMS-007-D02

Task Title: MODELISATION OF IRRADIATION EFFECTS AB-INITIO DEFECT ENERGY CALCULATIONS IN THE Fe-He AND Fe-He-C SYSTEMS

INTRODUCTION

Ferritic steels are proposed as structural material in fusion reactors. When subject to 14 MeV neutron irradiation, large amounts of helium and hydrogen are produced from transmutation in addition to self-defects. High He concentrations in metals are known to induce microstructural changes such as bubble formation and void swelling. The objective of this subtask is to contribute to the modeling of such phenomena by providing a database at the ab-initio level, i.e. in the framework of the Density Functional Theory (DFT), of energies and structures for a set of characteristic atomic configurations involving helium atoms, carbon, vacancies and self-interstitials in the α-Fe lattice. The present calculations are based on a fast DFT-code, namely SIESTA (Spanish Initiative for Electronic Simulations with Thousands of Atoms: http://www.uam.es/siesta) [1], [2]. This methodology was set up and validated in 2003 by comparison with reference calculations based on plane-wave basis sets [3]. It has been applied in 2004 to predict the migration of interstitial and substitutional He atoms in pure α-Fe, and their interaction with other He atoms and with vacancies. In 2005, this approach has been extended to the interaction between self-interstitials and He, and to the effect of carbon on the energetics of helium-vacancy clusters.

2005 ACTIVITIES

The results presented below are obtained at constant pressure, on 128 atom supercells, using 3x3x3 k-point grids for the Brillouin zone integration. All calculations are performed in the spin polarized Generalized Gradient Approximation (GGA).

INTERACTION BETWEEN HELIUM AND SELF-INTERSTITIALS

Interaction between interstitial He and self-interstitials

Helium atoms produced by irradiation are initially in interstitial sites of the iron matrix. According to ab-initio results an interstitial helium (He_{int}) prefers to be in tetrahedral rather than octahedral site and it migrates almost athermally with an activation energy of 0.06 eV [3]. It can then be obviously deeply trapped by a vacancy and become a substitutional impurity. However we have considered here the alternative where the interstitial helium atom finds a self interstitial atom before it is trapped by a vacancy. We have therefore calculated the interaction energies between a tetrahedral interstitial He and a <110> dumbbell - the most stable mono-interstitial configuration - for various relative positions of the two defects. We find that several of them are attractive; three of them are shown in figure 1. The most favorable situation found is when the He atom resides in a third nearest tetrahedral site of the dumbbell (figure 1 (a)). The corresponding binding energy is 0.26 eV and the dissociation energy - obtained by adding the migration energy of interstitial He - is 0.32 eV. However self-interstitial atoms can act as efficient traps only at temperatures where they are weakly mobile since their migration energy is ~0.3 eV. This will be the case only at relatively low temperatures.

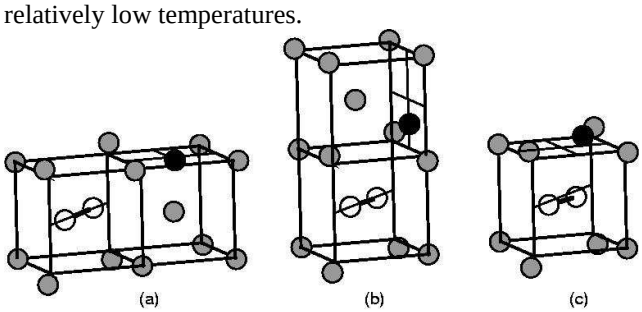

Figure 1: Schematic representations of (meta)-stable configurations containing a <110>dumbbell and an interstitial He at various tetrahedral positions. The black, gray and white spheres symbolize the He atom, the Fe lattice atoms, and the <110> Fe dumbbell respectively. The atoms are at their relaxed positions.

Interaction between substitutional He and self-interstitials

When a self-interstitial atom (I) approaches a substitutional He (He_{sub}) a spontaneous recombination-replacement (kick-out) reaction is expected to occur. We confirm here that the $He_{sub} + I \rightarrow He_{int}$ reaction implies a large energy gain, namely 3.6 eV. In other words the energy gained by recombining a Frenkel pair (5.9 eV) largely overcomes the energy lost by putting a helium atom from a substitutional to a tetrahedral site leaving an empty vacancy behind (2.30 eV). What happens before this reaction actually occurs - i.e. when the two defects are close to each other without the self-interstitial atoms spontaneously kicking the helium atom out of the vacancy - may also be important. We have therefore investigated such configurations by considering first the interaction between a He_{sub} and a <110> dumbbell. The kick-out reaction occurs spontaneously when a He_{sub} is at the nearest neighbour site within a (110) plan containing the dumbbell (figure 2 (a)), but when the He_{sub} is out of the plan (figure 2 (d)) a non negligible energy barrier prevents the spontaneous recombination. In this configuration a binding energy of 0.24 eV is found. From such a

metastable configuration the <110> dumbbell may perform usual translation-rotation jumps [2]. We have investigated one of them by considering the final configuration where the He_{sub} and the dumbbell are third neighbours (figure 2 (e)) which has a binding energy of 0.16 eV. The corresponding migration energy is 0.4 eV, i.e., slightly larger than the migration energy of an isolated <110> dumbbell (0.34 eV). Jumps similar to this one, i.e. between this type of metastable configurations, are likely to occur only if none of the migration barriers leading to kick-out processes are significantly lower, which remains to be investigated. These preliminary results show that one cannot exclude that a <110> dumbbell is temporally trapped by a substitutional He before the kick-out reaction occurs.

The situation may be similar in the di-interstitial case (two parallel <110> dumbbells). The most stable complex formed by the reaction of a di-interstitial with a substitutional He has an energy lower by 3.1 eV than that of the two isolated defects. As in the single interstitial case, we have found a metastable configuration with the two defects close to each other but without spontaneous recombination (figure 2 (f)), the corresponding binding energy is 0.52 eV.

The <111> dumbbell is 0.7 eV higher in energy than the <110> dumbbell according to ab-initio calculations [R2]. However this relative stability may change in presence of helium. We have therefore performed calculations with a <111> dumbbell close to a He_{sub}. We find that a recombination-replacement reaction occurs spontaneously for the two closest configurations (figure 2 (b) and (c)).

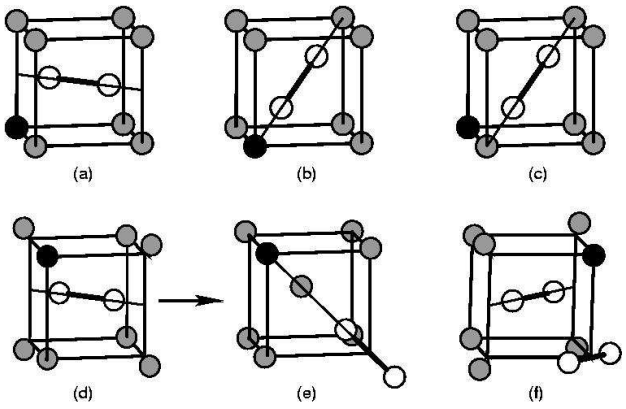

Figure 2: Schematic representations of systems containing a substitutional He and a mono- or a di-interstitial: configurations (a), (b), and (c) are unstable against a kick-out reaction while (d), (e) and (f) are local minima. (d) and (e) represent the initial and final positions of a <110> dumbbell performing a translation-rotation jump in the neighbourhood of a substitutional He.

EFFECT OF CARBON ON THE ENERGETICS OF HELIUM-VACANCY CLUSTERS

Effect of carbon on the binding energy of helium-vacancy clusters

Although carbon is present only in very small quantities in steels, it is expected to have a crucial effect on defects. Carbon indeed interacts strongly with vacancies in iron, as attested by the radical change on the apparent vacancy migration energy between ultra-pure iron, and carbon containing 10 appm of carbon or more. For this reason we have investigated the effect of carbon on the energetics of He_nV_m helium-vacancy clusters. The reactions selected as representative of these effects are summarized in table 1.

The comparison between reactions (1) and (1') shows that a single carbon atom has a relatively weak effect on the binding energy between a vacancy and He_{int}, the binding energy of He_{int} with a carbon vacancy complex and and He_{int} being only 0.21 eV lower than that with a pure vacancy. The formation of HeV_2 cluster shows an example with a lower n/m ratio. The effect of carbon is very large with a decrease of more than 1 eV of the binding energy (reactions (2) and (2')). In the same way when the n/m is decreased, the effect of carbon becomes weaker (reactions (3) and (3')). The general conclusion is therefore that the larger the n/m ratio, the weaker the effect of carbon.

On the other hand, the binding energy drops by more than one eV when a second carbon atom is added to the complex (see reaction (1")).

We have also investigated the effect of a second carbon atom in the cluster. This effect is large when comparing the binding of He_{int} to VC with that to VC_2.(reactions (1') and (1") respectively). The decrease by more than 1 eV of the binding energy may be attributed to the breaking of the C-C bond by the He atom. Adding a second He atom to these clusters gives approximately the same binding energy independently of the number of C atoms (reactions (3), (3'), and 3")). No C-C bonds are formed in this case.

Table 1: Summary of the main reactions investigated between helium (He), vacancies (V), and carbon (C). He_{int} and C_{int} denote interstitial helium and interstitial carbon, which are respectively on octahedral and tetrahedral sites. The energy balances of these reactions, i.e. the binding energies between the initial species are given in eV.

Reaction	Binding Energy (eV)
(1) $V + He_{int} \rightarrow HeV$	2.30
(1') $VC + He_{int} \rightarrow HeVC$	2.09
(1") $VC_2 + He_{int} \rightarrow HeVC_2$	0.94
(2) $V_2 + He_{int} \rightarrow HeV_2$	3.33
(2') $V_2C + He_{int} \rightarrow HeV_2C$	2.25
(3) $HeV + He_{int} \rightarrow He_2V$	1.84
(3') $HeVC + He_{int} \rightarrow He_2VC$	1.73
(3") $HeVC_2 + He_{int} \rightarrow He_2VC_2$	1.94
(4) $He_2V + C_{int} \rightarrow He_2VC$	0.02
(4') $He_2VC + C_{int} \rightarrow He_2VC_2$	-0.18
(5) $HeV + C_{int} \rightarrow HeVC$	0.14
(6) $HeV + V \rightarrow HeV_2$	0.78
(7) $HeVC + V \rightarrow HeV_2C$	0.58
(8) $HeV_2 + C_{int} \rightarrow V_2HeC$	0.00

Effect of carbon on the migration of substitutional helium by the vacancy mechanism

The dominant mechanism for the diffusion of substitutional He, i.e. the HeV complex, in the regime of excess of vacancies is the vacancy mechanism, which requires an incoming vacancy. We tried to estimate how the migration energy of this complex determined in 2004 to be 1.1 eV could be affected by the presence of carbon. According to binding energies associated with reactions (5-8) the carbon atom will most likely weakly affect the vacancy migration mechanism, since the binding of carbon to HeV and HeV_2 is quite weak. The emission of carbon from the cluster is indeed more favorable than that of its migration (without carbon), with respective energies of 0.87 eV and 1.1 eV. So even if the HeV_2C complex cannot migrate without dissociating, the presence of carbon is expected to only slightly delay the migration of the cluster. Kinetic simulations are required to give a more quatitative answer.

CONCLUSIONS

The following conclusions can be drawn from the present ab-initio calculations on the interaction of helium with self-interstitials in pure α-Fe and on the effect of carbon on helium-vacancy clusters:

- We have evidenced configurations with an attractive interaction between an interstitial He and a self-interstitial, with binding energies up to 0.3 eV.

- Substitutional He and self interstitial have a very strong tendency to form an interstitial He (the so-called kick-out mechanism which releases ~3.6 eV), but metastable configurations of close pairs of these defects have also been evidenced.

- Carbon has been shown to have the following effect on the binding of interstitial He with He_nV_m clusters: a rather weak effect for n=0 and m=1, but this effect strongly increases with decreasing n/m ratio. The effect of a second carbon atom depends strongly on the possibility to form C-C bonds.

- The effect of carbon on the migration mechanism of substitutional He by the vacancy mechanism is estimated to be rather weak, in view of the small value of the binding energy of C with HeV and HeV_2 complexes.

REFERENCES

[1] J.M. Soler, E. Artacho, J.D. Gale, A. Garcia, J. Junquera, P.Ordejon and D. Sanchez- Portal, J. Phys. Cond. Matter 14, 2745 (2002).

[2] C.C. Fu, F. Willaime and P. Ordejon, Phy. Rev. Lett. 92, 195503 (2004).

REPORTS AND PUBLICATIONS

[1] C. C. Fu and F. Willaime, *Ab-initio study of helium in α-Fe: dissolution, migration and clustering with vacancies*, Phys. Rev. B 72, 064117 (2005).

[2] C. C. Fu and F. Willaime, *Interaction between helium and self-defects in iron from first principles*, submitted for publication.

TASK LEADER

François WILLAIME

DEN/DMN/SRMP
CEA-Saclay
F-91191 Gif-sur-Yvette Cedex

Tel. : 33 1 69 08 43 49
Fax : 33 1 69 08 68 67

e-mail : francois.willaime@cea.fr

Not available on line

Not available on line

Not available on line

Not available on line

Not available on line

Not available on line

Not available on line

Not available on line

Not available on line

Not available on line

TW5-TTMS-005-D01

Task Title: RULES FOR DESIGN, FABRICATION, INSPECTION UPDATE DATA BASE AND APPENDIX A OF DEMO-SDC

INTRODUCTION

Eurofer is a reduced activation ferritic / martensitic steel that has been selected as the European reference structural material for ITER Test Blanket Modules and DEMO reactor. Several industrial heats of this steel have been produced and tested under EFDA's Tritium breeding and materials field / materials development tasks. The ultimate goal of these tasks is to propose materials properties allowable for design and licensing of components that will be fabricated with the Eurofer steel.

This report presents a summary of the work done during the year 2005 at CEA for the TW5-TTMS-005-D01. The work done is also part of an international collaboration, coordinated under the fusion materials implementing agreement of the International Energy Agency (IEA). The main objective of the TW5-TTMS-005-D01 is to collect, validate and harmonize the results of Eurofer steel, in continuation of the earlier work done on the conventional 9Cr-1Mo steel and the RAFM steel grade produced in Japan (F82H), and propose materials properties allowable through an Eurofer steel dedicated Appendix A.

2005 ACTIVITIES

All actions and deliverables foreseen under the terms of TW5-TTMS-005-D01 have been fulfilled in time. In 2005, the database of Eurofer steel was updated, particularly with the RAFM data and analysis resulting from the work done at CEA and NRG.
With the addition of the new Eurofer steel data in 2005, the collection of relational databases for RAFM steels contains:

- Products database: 571 records including 118 on Eurofer
- Compositions database: 475 records including 26 on Eurofer
- Tensile database: 1185 records including 258 on Eurofer
- Impact database: 1710 records including 467 on Eurofer
- Impact plots: 161 records including 45 on Eurofer
- Creep database: 205 records including 81 on Eurofer
- Fatigue database: 232 records including 70 on Eurofer
- Fracture toughness database: 261 records, mostly for Eurofer steel, including 8 Master Curves.
- A few fatigue crack propagation test results
- Summary records for all databases

Runtime CD-Rom version 5, linking all above databases and Appendix A reports, is also issued.

The content of the Appendix A is now well enriched with data on EB, TIG and diffusion bonded joints allowing a comprehensive evaluation of these joints along with the base metal (see e.g. figure 1). Also with the availability of high dose irradiation results precision of extrapolation of mechanical properties to higher doses is increased (see e.g. figure 2).

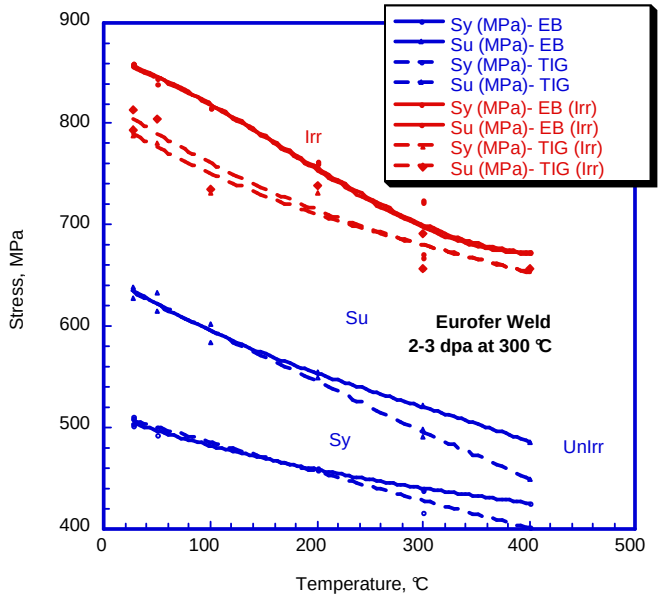

Figure 1: Effect of irradiation (2-3 dpa at 300°C in HFR, SUMO-03) on tensile yield and UTS of Eurofer weld metals, PWHT 1 h at 720° C (NRG data)

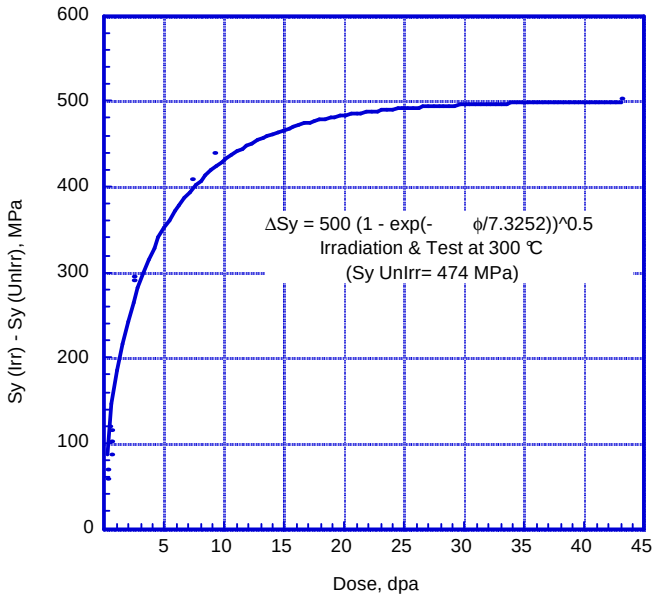

Figure 2: Effect of irradiation at 300 °C on yield stress of Eurofer steel tested at 300 °C (ΔS_y versus dose in dpa, including CEA high dose data)

CONCLUSIONS

Appendix A for Eurofer steel and its various types of joints is now well established. It will be further improved in 2006 with data from even higher doses. For 2006 and beyond a report on ODS version of this steel is proposed.

REPORTS AND PUBLICATIONS

F. Tavassoli, "Fusion Interim Structural Design Criteria (DISDC), Appendix A Material Design Limit Data: A3.S18E Eurofer Steel", TW5-TTMS-005-D01, CEA/DMN/Dir/2005-01/A, to be issued Dec. 2005.

TASK LEADER

Farhad TAVASSOLI

DEN/DMN
CEA-Saclay
F-91191 Gif-sur-Yvette Cedex

Tel. : 33 1 69 08 60 21
Fax : 33 1 69 08 80 70

e-mail : tavassoli@cea.fr

TW5-TTMS-006-D01

Task Title: STRUCTURAL MATERIALS - HIGH PERFORMANCE STEELS IMPROVEMENT OF FABRICATION PROCESS FOR ODS-EUROFER - REFINEMENT OF CHEMICAL COMPOSITION AND THERMOMECHANICAL TREATMENTS WITH EMPHASIS ON THE FABRICATION ISSUES OF LARGER BATCHES

INTRODUCTION

Compared to HIP, hot-extrusion process presents the advantage to induce a more homogeneous and finer microstructure without porosity, favourable features to optimize the material's performance and in particular to decrease DBTT values.

The main objectives of this task are to assess the process of hot-extrusion to obtain ODS-EUROFER with improved DBTT and to compare the effect of the yttria content (0.3 and 0.5%) on the tensile and impact properties of hot-extruded ODS-EUROFER alloys.

2005 ACTIVITIES

The compaction by hot-extrusion was applied to mechanically alloyed powders of EUROFER with yttrium oxide contents of 0.3 and 0.5 wt % (supplied by FZK), which have been extruded at 1100°C as rod bars of 13 mm in diameter and rectangular bars of 7.7 mm thickness and 24 mm width.

A homogenisation treatment at 1050°C during 15 min followed by a slow cooling has been applied to the rod bars. Rectangular bars have been cold rolled to 30% reduction in thickness then heat treated with the same conditions of time and temperature than the rod bars.

Tensile cylindrical specimens of 2 mm in diameter and 12 mm of gauge length and Charpy V-notch subsize specimens were machined in the longitudinal direction of the bars.

Mechanical tests are in progress.

First results on impact properties of ODS-0.3% Y_2O_3 were obtained by Charpy tests performed over the range temperature –100 to +320°C to produce the full energy transition curve (figure 1). The Ductile-Brittle Transition Temperature (DBTT) evaluated by means of the hyperbolic tangent method is about –40°C.

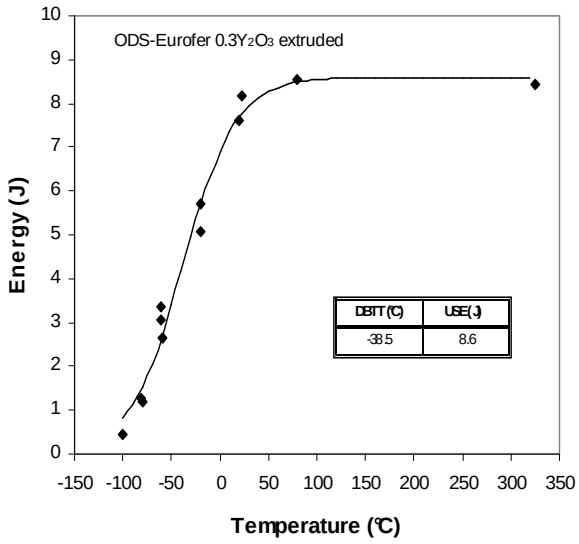

Figure 1: Evolution of absorbed energy as a function of

CONCLUSIONS

The first results of Charpy impact tests performed on extruded material containing 0.3% Yttria confirm the better value of DBTT (-40°C) and the higher level of the upper shelf energy (about 8.6 J) compared to the same material obtained after consolidation by HIP.

TASK LEADER

Annick BOUGAULT

DEN/DMN/SRMA/LA2M
CEA-Saclay
F-91191 Gif-sur-Yvette Cedex

Tel. : 33 1 69 08 54 45
Fax : 33 1 69 08 71 30

e-mail : annick.bougault@cea.fr

TW5-TTMS-007-D04

Task Title: MODELISATION OF IRRADIATION EFFECT EVENT-BASED MONTE CARLO SIMULATIONS OF DEFECT MICROSTRUCTURE EVOLUTION OF IRON CONTAINING C DURING RESISTIVITY RECOVERY EXPERIMENTS

INTRODUCTION

The objective of the work is to study the defect accumulation and microstructure evolution in Fe containing carbon (C). The latter is known to strongly affect the mobility of defects created during irradiation (interstitials and vacancies) and has therefore a direct consequence on the material microstructure evolution.

Resistivity recovery experiments conducted with carefully controlled C contents were performed by Takaki as soon as 1983 [1]. To explain the various recovery stages, he invoked the intervention of individual point defects, defect clusters and solute+defect clusters having that very migration (or binding) energy to promote the corresponding resistivity recovery at the temperature under examination. The resistivity technique being macroscopic in essence, it could yield only a complicated average of a large number of elementary processes; but there was at that time no tractable tool to control the conclusions. These proposals were, at that time, the most reasonable ones, taking due account of the rather crude state of the art concerning the calculation of defect energetics.

The point of view changed in the last decade since the onset of ab-initio methods which provide us today with confident (if not perfect) values of the energies of elementary events made up by the formation, the migration, the association and dissociation of defects. In pure BCC iron, the following energies were found [2]: the migration energy of the single vacancy (V) is 0.67 eV, while the binding energies of di-vacancies V2 , tri-vacancies V3 are 0.3 eV and 0.37 eV and their migration energies are 0.63 eV and 0.35 eV respectively. The migration energy of self interstial (I) amounts to 0.34 eV while the binding energies of I2 , I3 are 0.80 eV and 1.4 eV and their migration energies are 0.42 eV and 0.43 eV respectively.

On the other hand Monte Carlo simulations are currently reaching that state where the simulated volume of matter approaches the experimental one and where the time scale which can be probed, although still limited, becomes closer and closer to the one probed under the experimental conditions. The kinetic Monte Carlo method Jerk, developed in Saclay presents unique capabilities: it rests upon a detailed knowledge of elementary atomistic mechanisms and takes advantage of rate theory, it can handle rare events which play a key role in the nucleation process of complex clusters [3]. Using the small number of ab-initio data quoted above as input parameters, it was successfully used to explain the resistivity recovery changes of pure iron under electron irradiation [2].

The challenge is now to extend this approach to the case of iron containing carbon.

At the start of this work, three main deliverables were planned as follows:

* M1: parametrization of carbon doped iron (interactions of C with self defects and defect clusters)

* M2: application to resistivity recovery of carbon doped iron after a low temperature e- irradiation (influence of dose and carbon content) + parallelization of Jerk

* M3: final report

The death of the principal investigator at the beginning of 2005 slowed the work, which was restarted in december 2005. Point 1 is the principal result obtained in 2005; points 2 and 3 will thus be the output for 2006.

RESULTS OF STEP M1

The first step was done in relationship with task TW4-TTMS-007-D02: ab-initio calculations are required for the migration and stability of the defects which are used as input data in the Monte Carlo simulations. New parameters relevant to carbon doped iron were calculated with the Siesta code (DFT + GGA approximation; spin polarized calculation; pseudo-potentials, pseudo atomic orbitals). The calculations were conducted on supercells containing 128 atoms (relaxation of force and stress tensor, migration path investigated with the drag method). The main results can be summarized as follows:

- C atom resides in octahedral interstitial sites; the energy barrier for migrating from an octahedral site to a neighboring one is 0.87 eV, in excellent agreement with experiments (and similar evaluations performed with other ab-initio codes).

- C attracts vacancies and promotes the formation of complexes VC, VC2, V2C, V2C2; with positive binding energies (0.41 eV, 1.18 eV, 0.83 eV, 1.40 eV respectively). At larger sizes, the effect of carbon seems to be less favourable. As a consequence only these complexes will be considered in the simulations. All of them are assumed immobile, but they can emit mobile species. The difficult point is the multiplicity of possible decomposition paths for each of them. Denoting each possible reaction followed by the dissociation barrier to be overcome yields:

VC --> V + C	0.41 + E_m(V)
V_2C --> VC + V	0.42 + E_m(V)
V_2C --> V_2 + C	0.53 + E_m(V_2)
VC_2 --> VC + C	0.77 + E_m(C)
VC_2 --> C_2 + V	1.18 + E_m(V)
V_2 C_2 --> VC_2 + V	0.22 + E_m(V)
V_2 C_2 --> V_2C + C	0.57 + E_m(C)

Where E_m(d) is the migration energy of defect 'd'. For obvious energetic reasons, the path which is favoured is the one involving the lowest activation barrier.

- C attracts interstitials and promotes mainly the formation of immobile complexes I C, I_2C and I_3C (binding energies euqal to 0.12 eV, 0.87 eV, 1.52 eV respectively). The binding energy increases with the size but some assumption must still be made for including the asymptotic behaviour at larger sizes. Only the following reactions are considered:

IC --> I + C	0.12 + Em(I)
I_2C --> I_2 + C	0.19 + Em(I_2)
I_2C --> IC + I	0.87 + Em(I)
I_3C --> I_2C + I	0.53 + Em(I)
I_3C --> IC + I_2	0.60 + Em(I_2)
I_3C --> C + I_3	0.22 + Em(I_3)

Where the migration energies of interstitials were quoted above.

- C-C interaction is slightly repulsive at first and second neighbour distances. But knowing that the presence of carbon promotes the formation of cementite Fe3C or ε-carbide, some attraction at a larger distance must be invoked. This point is delicate and has very important consequences on the formation of C clusters in the C doped iron samples: the path for nucleating larger C clusters will not be the same if C2 can be considered as a possible nucleus for cementite or if other reactions must be invoked.

RESULTS OF STEP M2

As a first pre-requisite, we had to parallelize the code cut down the computer time. This has been performed efficiently by distributing on several CPU's the most time consuming step in the calculation, namely the building and book-keeping of the table sorting the events (encounters of mobile partners, dissociation events ...etc) in the order of increasing delays of occurrence. The obtained speed up is reasonable but depends noticeably on the temperature (higher at lower T) because of a different balance between the number of reaction events to be considered and the latency attached to the sending of messages:

- at the higher temperatures (350 K and above) the number of reacting defects is small: the time spent in the subroutine calculating the delays is not large enough when compared to the time spent in message passing. The speed up amounts to 10 with 8 processors (over speed up due to data entirely contained in the cache size) and only to 12 for 16 processors. As a consequence, the number of 10 processors seems optimal.

- at lower temperatures (100 K and below), the number of defects and the number of reaction events to be considered is much larger than before, but many of them do not happen and can be rapidly cancelled out because of the low mobilities. The longer time spent in the calculation of delays is not too much altered by the time spent in message passing, and a speed up of 22 was obtained with 30 processors. Some more gain can be expected with more than 30 processors.

The second step consisted in implementing in the code all the new mechanisms listed above and in studying their influence on the resistivity recovery curves. Only preliminary results are available today but they look encouraging:

- new peaks are obtained which correspond to the migration or dissociation of new entities in agreement with experiments (carbon migration above 350 K, dissociation of VC and VC2 complexes above 570 K) [1].

- the interpretation of irradiation dose effect is more complicated than for the case of pure iron, where a larger dose implied shorter distances between reaction partners and thus a simple shift of the recovery peaks at lower temperatures. Conversely, for carbon doped samples, the positions of these new recovery peaks depend now on two independent parameters, the irradiation dose and the initial C content: indeed, these new peaks are monitored by the relative amounts of C atoms and individual defects which have survived. Their concentrations are ruled by many more reactions than without carbon.

- at last the approximation used-up to now for calculating the resistivity must be revised. For pure iron, the resistivity of a cluster containing n defects was evaluated as the sum of the resistivities due to each defect. For carbon doped iron, this linear rule had to be modified by assuming that the resistivity of the cluster containing p defects CI_n CV_n C_nI_m and C_n varies as $p^{2/3}$ to get reasonable amplitudes for the recovery peaks.

REFERENCES

[1] S. Takaki et al. , Rad. Effects 79 (1983) 87.
[2] C.C. Fu et al. Nature Mat. 4 (2005) 68.
[3] J. Dalla Torre et al., Phil. Mag. 85 (2005) 549.

TASK LEADER

Jean-Louis BOCQUET and L. JOLY

DEN/DMN/SRMP
CEA-Saclay
F-91191 Gif-sur-Yvette Cedex

Tel. : 33 1 69 08 54 62
Fax : 33 1 69 08 68 67

e-mail : jean-louis.bocquet@cea.fr

TW5-TTMS-007-D21

Task Title: STRUCTURAL MATERIALS - MODELISATION OF IRRADIATION EFFECTS FUSION-RELEVANT MATERIALS IRRADIATION IN JANNUS FOR MULTI-SCALE MODELLING EXPERIMENTAL VALIDATION

INTRODUCTION

The progress made in the understanding of the radiation damage physics and the increase of the computing capabilities has allowed for developing multi-scale computer tools to predict the radiation damage in pure metals and dilute alloys. These tools have been considered to be matured enough to attempt to extend them to more complex industrial materials [1].
On this basis a modelling activity is supported by EFDA with the main following objectives reprinted from reference [1]:

"To study the radiation effects in the EUROFER reduced activation ferritic-martensitic steel under fusion relevant conditions in the range of temperatures from RT to 550°C in the presence of high concentrations of nuclear derived impurities (i.e. H, He).

For such purpose, the tools and database to correlate results from fission reactor - spallation source – fusion neutron source should be developed as well as the extrapolation to high fluence. Of particular interest are the effects of:

- Chemical composition and the role of different alloying elements as well as that of the impurities produced through nuclear reactions such as H and He.

- Microstructure, particularly in terms of the different boundaries present.

- Mechanical properties: role of irradiation and impurities on hardening, embrittlement, and fracture.

It should be emphasized that the models and the tools derived from them should be validated experimentally".

Ion irradiation has been proven for the past thirty years to be particularly effective and flexible in studying irradiation effects in well controlled irradiation conditions at low cost and with rapid feedback. The volumes of radiation-induced microstructure accessible to multi-scale modelling are presently comparable to those that can be irradiated via ion beams and physically-chemically characterized by the different available techniques (TEM, FEGSTEM, IBA, AP-FIM, Synchrotron light). In addition, recent progresses in miniaturized specimens for mechanical testing, including post-mortem nano-indentation and in-situ TEM testing will make possible to get the relevant data for the dislocation dynamics in microstructure induced via ion irradiation.

Therefore the coupling of multi-scale modelling, ion-irradiation and characterization will provide an effective way in defining, carrying out and interpreting the critical experiments required to develop and validate the modelling tools that are necessary to interpolate the data obtained with various neutrons sources, to optimize the future irradiation programme in IFMIF and extrapolate all these data to the varied operating conditions of the in-vessel components of a Fusion reactor.

In the next two sections we describe the general objectives and strategy of the experimental program in Jannus. Detailed explanations of the different tasks that should be pursued in the experimental program coupled with simulations to elucidate specific phenomena, such as configuration, (i) migration, clustering of point defects and He, (ii) kinetic pathway for high dose and high concentration of He and H and (ii) mechanical behaviour are not given here. They are too long to be presented here. They constitute sections 4 to 7 of the full 22 pages report available on demand.

OBJECTIVE

The purpose of this task is the redaction of a document describing the experimental strategy for the validation and verification of the multi-scale modelling approach using the multi-beam ion facilities JANNUS that will be operative at Saclay and Orsay in 2007. The strategy includes proposals by CEA, EPFL, UKAEA, Oxford and Alicante university. Have participated to the redaction: R. Schaeublin (EPFL), M. J. Caturla (UAAP), A. Barbu (CEA), S. Dudarev (UKAEA), P. Vladimirov(CEA) and J.L. Boutard (CEA)

2005 ACTIVITIES

EXPERIMENTAL STRATEGY

Objectives of the experimental programme in Jannus

The objective of Jannus is to provide the test–bed for modelling oriented experiments to build and validate the multi-scale modelling of the microstructure kinetic evolution and the associated dynamics of dislocations. The experimental programme will address for the selected reference materials:

- the point defect behaviour and their diffusion

- the primary irradiation damage essentially the cascade development and recovery

- the kinetic pathway of microstructure evolution to high dose: point defect clusters, precipitates, segregation, void swelling

- the consequences of the microstructure on the in-service properties: mechanical properties (plasticity and visco-plasticity).

The reference materials are for DEMO the following ones: Eurofer & ODS ferritic/martensitic steels for the structural materials, and, tungsten for the armour materials, with the first priority given to Eurofer in agreement with the modelling programme.

The document will present first elements of strategy followed to build the experimental programme.

Then the description of the programme will be organized as followed:

- Point defect behaviour: configuration,

- migration, clustering

- Kinetic pathway of the microstructure to high dose

- Under irradiation phase stability

- Dynamic of dislocations in radiation induced microstructure

- In-beam creep

Table I gives, reprinted from [1], the modelling tools with a short description and the deliverables expected from the modelling programme.

Strategy for modelling-oriented experiments

The strategy depends on the response of the considered material to irradiation, and, the maturity and the reliability of the modelling prediction.

Eurofer martensitic steel:
Point defects, microstructure at high dose high He and H concentrations

Eurofer is a martensitic steel with ~9% Cr the radiation induced microstructure of which is determined by the clustering of point defects and He&H produced by the neutron irradiation.

The recent multi-scale prediction of electron damage recovery in ultra-pure α-Fe based on ab-initio calculations of the formation and migration energies of point defect clusters [2] as well as the progress made in the ab initio prediction of the cohesive and kinetic parameters governing the behaviour of He in presence of point defects [3] make the objective of an ab initio based multi-scale modelling of the radiation induced microstructure most probably achievable in the next five years within the Fusion Material Modelling Programme for dilute alloys such as $\tilde{\alpha}$Fe-C-He.

Table 1

Method	Description	Deliverable Object
Ab-initio	Potential	Bcc Fe potential
Ab-initio	Calculation of binding energies & jump frequencies	He-vacancy binding energy
MD	Displacement cascades	Type of defect resulting from cascade Evolution of cascade in the presence of He
MD (and statics)	Evaluation of the dislocation -defect interactions	Dislocation-defect interaction at the atomistic level as input for DD calculations
MD	Interaction of cascades and defects with grain boundaries	Effect of GB on cascade evolution. Evaluation of sink strength
Lattice KMC	Cohesion & diffusion model	Phase stability
kMC, OKMC, EKMC (Jerk)	Early stages of defect (and solutes) evolution	Early stages of microstructure evolution
Analytical modelling (Rate Theory)	Later stages of defect (and solutes) evolution	"Steady State" time-temperature microstructure evolution
DD	Calculation of the interaction between defects and a distribution of dislocations	Initial hardening, strain localization
DD + FEM	Calculation of the interaction between defects and a distribution of dislocations	Evolution of the deformation microstructure: work hardening
DD + FEM	Stress-strain singularities and crack propagation	Fracture properties

Conversely it is well known that the initial microstructure and chemical composition control in a complex manner the radiation effects in industrial materials so that it is most probably out of reach within the five forthcoming years to multi-scale model such materials without some adjustable parameters, tuned as much as possible on dedicated experiments and on the knowledge gained from experiments and physical modelling on simpler systems.
Therefore the strategy for the Jannus experimental programme in support to the multi-scale modelling of radiation induced microstructure for Eurofer will be to select a few relevant chemical compositions of increasing complexity with the following rationale:

- Study a few simple model alloys: Ultra-High Purity (UHP) α-Fe and UHP α-Fe doped with C for which the radiation damage, point defect and He accumulation, can be modelled from well-defined physical data obtained from ab initio and assessed via the experiments dedicated to point defect behaviour, i.e. without tuneable parameters. These materials should be well annealed to have the simplest initial microstructure.

- Study a few model alloys such as UHP α-Fe-Cr, UHP α-Fe-C-Cr, α-Fe-C-Cr-W. The chemical composition is complex enough so that some parameters of the previously well-established models are to be tuned using the knowledge gained on the simple model alloys and the knowledge gained with Jannus on the point defect behaviour. The materials are also in annealed condition.

- Study the industrial material the chemical composition and the microstructure of which are more complex, and, rely on the documented method described above to propose the best set of parameters.

Eurofer ferritic/martensitic steels: from microstructure to mechanical properties

The yield properties of the non-irradiated 9 Cr martensitic steels of Eurofer type depend on the chemical composition, the martensitic lath dimension and dislocation density. This type of material has to be used in operating conditions that allow for the stability of carbides and martensitic lath structure. The radiation-induced clustering of point defects within the laths will strongly affect the plastic behaviour of Eurofer:

- For $T<0.45T_m$, the hardening will be due to the obstacle forces against the dislocation motion. In addition, the localisation of the plastic deformation ($T<0.3\ T_m$), the so-called channelling, has to be understood as it leads to premature failure.

- For $T>0.45T_m$, the issue is the effect of the radiation-induced microstructure on the creep strength.

- Under irradiation, irradiation creep mechanisms are operating the main issue is how they are affected by the microstructure and chemical composition.

The dynamics of dislocations that will control these phenomena depends very much on the chemical composition as well as the nature, size and density of the obstacles. The various α-Fe-based model alloys should offer a large range for these parameters. Therefore, as for microstructure, the strategy of model alloys is proposed to be used with three objectives:

- determine the obstacle forces of the obstacles via in situ TEM testing

- determine the collective behaviour of dislocations and occurrence of channelling via nano-indentation or mechanical testing of miniaturized specimens

- assess the irradiation creep via in-beam tests

It should be noted that the prediction of obstacle forces or reactions between dislocations and point defect clusters requires the simulation of millions of atoms, which are out of reach of ab-initio calculation. They are performed via Molecular Dynamics based on empirical inter-atomic potentials the predictability of which has to be carefully assessed. Progress is being carried out for more reliable potential in α-Fe and possibly for α-Fe-C in various laboratories and within the PERFECT project. As well Discrete Dislocations Dynamics codes are being developed for α-Fe in the thermally activated and athermal regime.
All these efforts associated with the one within the fusion-material modelling programme should contribute to a reliable DDD modelling of materials irradiated in fusion condition, and, give the physical basis for crystalline plasticity and continuum mechanics for the macroscopic plastic behaviour.

ODS ferritic steels:
Microstructure and mechanical properties

The ODS ferritic steels have been developed to have higher heat resistance because of (i) a dispersion of fine oxide particles for high strength and creep resistance at high temperatures and (ii) higher chromium content, typically ~14 % Cr, so that they do not suffer α>α' transformation. The price to pay is nevertheless the α/α' unmixing in two ferritic phases due to the phase gap in the Fe-Cr diagram.
The major issues are therefore, in addition to the point defect & He clustering like in Eurofer martensitic steels, the stability of the oxide particles under irradiation and He production, and, the evolution and characterization of the overall microstructure induced by the α/α' unmixing. The study of the α/α' unmixing may be performed on model alloys with varying the Cr content. The study of stability of the oxide particles and of the overall radiation induced microstructure, however, requires considering the industrial material in its complexity, initial chemical composition and microstructure with the various interfaces and sinks.
The consequences of the radiation-induced microstructure evolution on the mechanical properties, for example:

Table 2

Tasks	2006	2007	2008	Total
Point Defects: configuration, migration, clustering				
4.1 Modelling of SIA defects and clusters in a-Fe and a-Fe-Cr	1	1		**2**
4.2 Essessment of experimental techniques to characterise SIA clusters	1,5	1,5	1,5	**4,5**
4.3 Identification of SIA configurations, transitions and mobility in a-Fe	0,5	2	2	**4,5**
4.4 Identification of SIA defects in bcc non-magnetic transition metal: the case of W	0,5	2	2	**4,5**
4.5 Identification of He mechanisms in α-Fe	2	2	2	**6**
4.6 Effect of composition on irradiation induced defects in ferritic alloys	0,5	1	1	**2,5**
Sub Total	**6**	**9,5**	**8,5**	**24**
Kinetic Pathway of the microstructure to high dose and He & H contents				**0**
5.1.2 High dose microstructure of UHP α-Fe and α-Fe+C under dual beam	2	2	1	**5**
5.2.1 High dose microstructure of α-Fe-Cr-C-W model alloys and Eurofer under dual beam	2	2	1	**5**
5.2.2 High dose microstructure of Eurofer under triple beam	1	1	0,5	**2,5**
Sub-Total	**5**	**5**	**2,5**	**12,5**
Under Irradiation Phase Stability				**0**
6.1 Phase separationin Fe-9Cr, Fe-12Cr, Fe-14Cr and EUROFER	0,5	1	1	**2,5**
6.2 Phase stability of ODS ferritic steels	0	2	2	**4**
6.3 W alloys	0	0	0	**0**
Sub-Total	**0,5**	**3**	**3**	**6,5**
Mechanical Properties				**0**
7.1 Microscale Technology (MST) applied to ion implanted ferrous alloys	0	0,5	0,5	**1**
7.2 In-situ tensile testing of ion implanted ferritic alloys	0,5	0,5	0,5	**1,5**
7.3 Dislocation-defect interaction in pure α-Fe and Fe-Cr alloys	0,5	0,5	0,5	**1,5**
Sub total	**1**	**1,5**	**1,5**	**4**
TOTAL	**12,5**	**19**	**15,5**	**47**

- For T<0.45Tm, will an ODS steel with a matrix demixed into α/α' suffer from channelling when yielded at low temperature (T<0.3 Tm)?

- For T>0.45T_m, will the radiation modified particles still be strong obstacle to dislocation in the creep range?

- Under irradiation will the ODS still be effective in reducing creep straining controlled by irradiation creep mechanisms?

are questions that are not understood enough to be studied step-wise on model materials and need to be studied on the actual materials.

CONCLUSIONS

Table 2 summarizes the task and associated manpower. The time-schedule of the manpower is not optimized but the total is relevant.

REFERENCES

[1] M. Victoria, G. Martin and B. Singh, The Role of the Modeling of Irradiation Effects in metals in the European Fusion Materials Long Term Program.

[2] C. C. Fu, J. Dalla Torre, F. Willaime, J-L. Bocquet and A. Barbu, Nature Materials, vol. 4, p. 6 (2005),

[3] C. C. Fu and F. Willaime, Ab-initio study of Helium in a-Fe: dissolution, migration and interaction with vacancies.
Report DMN/SRMP/NT/2005-002/A.
Task TW4-TTMS-007.

TASK LEADER

Alain BARBU

DEN/DMN/SRMP
CEA-Saclay
F-91191 Gif-sur-Yvette Cedex

Tel. : 33 1 69 08 43 49
Fax : 33 1 69 08 68 67

e-mail : alain.barbu@cea.fr

TW3-TTMA-001-D04
TW3-TTMA-002-D04

Task Title SiC/SiC CERAMIC COMPOSITES AND DIVERTOR AND PLASMA FACING MATERIALS

INTRODUCTION

The objective of these tasks is to irradiate in a common rig SiC/SiC ceramic composites and tungsten alloys samples at two temperatures, i.e., 1000°C and a lower temperature approximately of 600-650°C. The dose foreseen is about fluence of 5.101 n.cm-2.5 dpa equivalent Fe.
This irradiation experiment will be performed in the OSIRIS reactor at CEA-Saclay.

The first step of this work consists on the design of the corresponding irradiation capsule based on the requirements defined by EFDA for this irradiation experiment, i.e., fluence level, temperature distribution, environment, materials, type, number and dimensions of specimens.
As said before, two families of materials are planned to be irradiated in this experiment, that is, several types of SiC_f/SiC ceramic composites and refractory tungsten-based alloys, all of them supplied by EFDA.

2005 ACTIVITIES

EFDA delivered the samples of W-alloys and SiC/SiC composite for this experiment, named "FURIOSO" (FUsion RIg OSiris irradiatiOn), during june-july 2005.

Materials were delivered as machined specimens ready for irradiation. All specimens were identified by laser engraving; also the dimensions of each individual sample were determined to proceed to the final distribution of specimens in different baskets. The final design of the irradiation capsule was adjusted to the actual dimensions of each sample.
The design of furnaces and gas circuit systems was finished and the fabrication of them as well as the irradiation capsule was launched in the 2nd half 2005.

LOADING PLAN

Table 1 presents the loading plan, which summarises the materials and the characteristics of specimens (type, dimensions and number) that will be irradiated in this experiment.
Different nuances of SiC-SiC ceramic composites are considered for irradiation: 2D and 3D-composites supplied by EFDA and manufactured in Europe by MAN Technology (Germany); 2D-NITE material from Japan and two types of composites supplied by ORNL (U.S.). These materials are included as specimens for mechanical tests (tensile and bending tests) and as samples for measurements of thermal diffusivity.

Concerning tungsten, two types of alloys will be included in the rig, one containing lanthanum oxide (W-1%La2O3) and other with potassium addition (W-K). These materials will be irradiated as plate tensile specimens and Charpy V subsize (KLST) samples destined to bending tests.

Table 1: Loading plan: distribution of different materials and specimens in the rig

			Composites SiC / SiC				W- alloys	
	Temp. (℃)	Basket #	EU-3D	EU-2D	J-NITE	US	W1	W2
TOP	600℃	1					5Ch+3T19	
		2						5Ch+3T19
		3	4Bend+ 5T45	5T45				
		4	4Bend	6Bend				
		5			8T40	8T40		
		6	5D10	5D10	5D6	5D6		
	Isolating region							
	1000℃	7	5D10	5D10	5D6	5D6		
		8			8T40	8T40		
		9	4Bend	6Bend				
		10	4Bend+ 5T45	5T45				
		11					6Ch+3T19	
BOTTOM		12						6Ch+3T19
			Total number of specimens					
T40 : Tensile 4x2x40					16	16		
T45 : Tensile 4x2x45			10	10				
Bend : 4x3.5x45			16	12				
D6 : Diffusivity 0 6x2.5 thick					10	10		
D10 : Diffusivity 0 10x2.5 thick			10	10				
Ch : Charpy KLST							11	11
T19 : Tensile 5x1x19							6	6

(dimensions in mm)

IRRADIATION RIG

The irradiation rig will be constituted of two capsules, one that will work at 1000°C and the other at 600°C. Figure 1 shows a scheme of one irradiation temperature section of the sample holder. Each section is constituted of six baskets to locate the samples. SiC/SiC composite specimens occupy four baskets and W- samples are distributed in the two others.

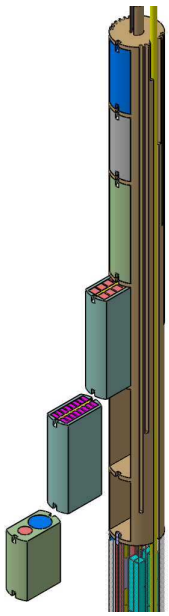

Figure 1: Scheme of one irradiation temperature section constituted by six baskets for the distribution of different types of specimens.

The same distribution and number of samples is considered for each irradiation temperature. Figure 2 presents the details of the six baskets constituting one irradiation-temperature capsule.
A mock-up of the assembly (baskets and holders), shown in figure 1, was manufactured to check the fitting of different components.

The main concern in the design was related to the temperature distribution in the device because the materials behaviour is strongly dependent on the irradiation temperature. This parameter depends on the rig's position in the reactor core (gamma heating), the

geometry of the sample holders, dimensions and shape of specimens.

A powerful furnace was designed, and the fabrication is in progress, to guarantee the regulation and control of specimen's temperature during irradiation. Besides the heating system, the temperature will be also regulated, using a flowing mixture of inert gas (helium-neon), inside and outside the sample holder that allows a better control and regulation of temperature.

N°	Kind of sample	Geometry	N.	Disposition of samples	Range of temperature
7	SiC	Ø6*2.5 Ø10*2.5	10 10	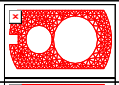	1000-1030°C
8	SiC	4*2*40	16	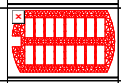	950-1020°C
9	SiC	4*3.5*45	10	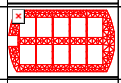	950-1010°C
10	SiC	4*3.5*45 4*2*45	4 10		960-1015°C
11	W	4*3*27 5*1*27	6 3	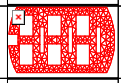	1050-1100°C
12	W	4*3*27 5*1*27	6 3	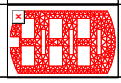	1020-1070°C

Figure 2: Geometry, dimensions and number of samples distributed in the capsule that will be irradiated at 1000°C. The same distribution is considered for the section at 600°C.

Consequently, inside the capsule, samples will be in contact with a circulating gas mixture of helium and neon.
The dimensions of all specimens were checked to adjust the foreseen distribution of samples and finalise the design of each sample-holder aiming to control the contribution of the gas gap responsible to the irradiation temperature.
The monitoring of temperature will be performed with thermocouples located in the sample holder.

FUTURE WORK

The fabrication of the irradiation capsule, the furnaces and the gas circuit systems were launched during 2005. Their delivery is expected in the 1st half 2006 and the start of the irradiation just after.

TASK LEADER

Ana ALAMO

DEN/DMN/SRMA
CEA-Saclay
F-91191 Gif-sur-Yvette Cedex

Tel. : 33 1 69 08 67 26
Fax : 33 1 69 08 71 67

e-mail : ana.alamo@cea.fr

TW5-TTMA-001-D08

Task Title: MODELLING OF THE MECHANICAL BEHAVIOUR OF ADVANCED 3D SiC_f/SiC COMPOSITE

INTRODUCTION

The work performed in 2005 consists in the implementation in CAST3M of two new constitutive laws adapted to SiC_f/SiC composite. These laws were developed at ONERA (French National Office for Aerospace Research). These new models, with convenient material parameters, obtained from 0° and 45° traction compression tests on woven SiC_f/SiC, allow to reproduce the experimental macroscopic behaviour of this composite. Comparison of CAST3M and ZeBuLoN (ONERA finite element code) results were performed.

2005 ACTIVITIES

SCALAR AND PSEUDO-TENSORIAL MODEL (CONSTITUTIVE LAWS)

Models developed at the ONERA allow taking into account various phenomena observed during ceramic matrix composite testing.

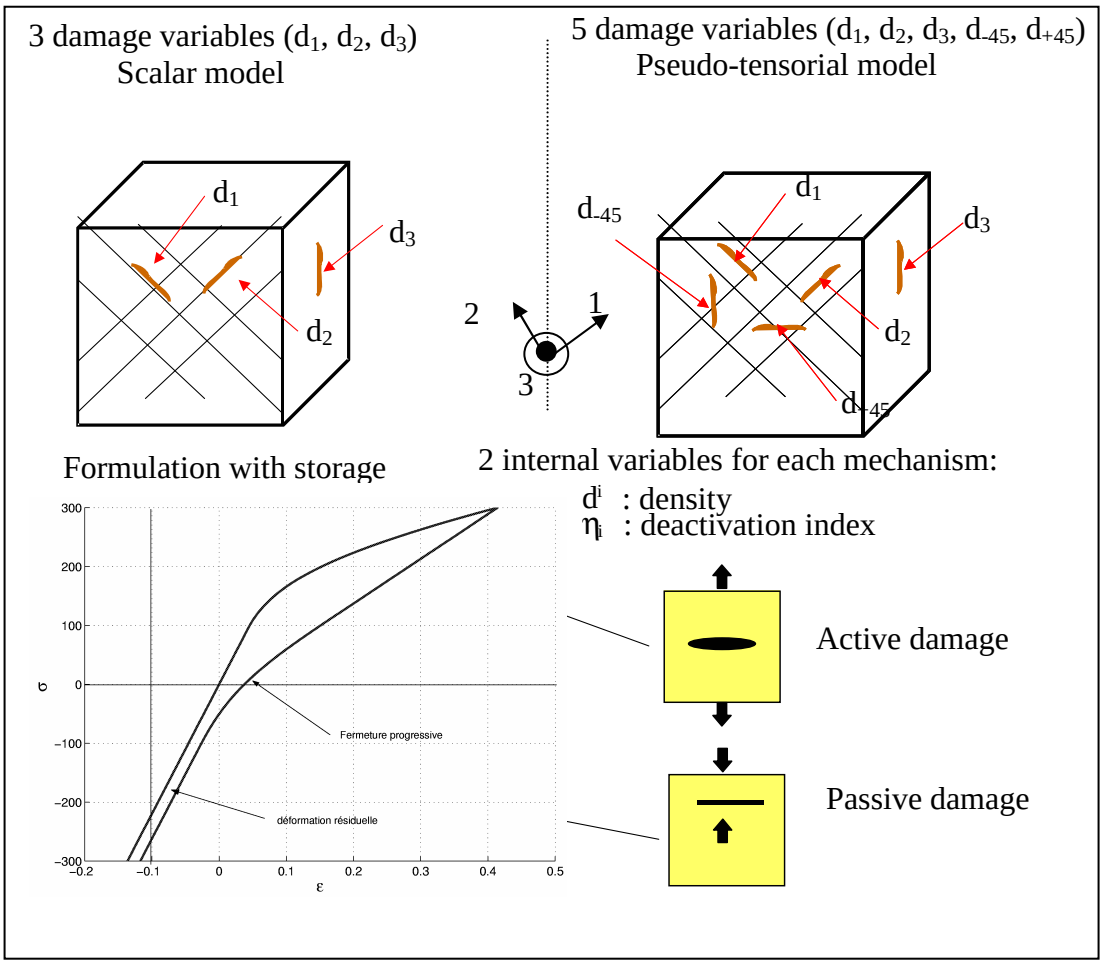

Figure 1: Different damage variables and main phenomena taken into account in the scalar and pseudo-tensorial models. Fibres are along directions 1 and 2

These models include:

i) the initial and damage induced anisotropy (with the eventual lost of orthotropy),
ii) damage kinetics for the different cracking modes (different cracks families defined by their orientations),
iii) damage deactivation and progressive cracks closure,
iv) residual strains induced by damage and residual fabrication stresses.

The damage variables can be defined as scalar, vector or tensors. In the case of ceramic matrix composites, the cracks directions depend on the material structure but also on the loading directions. For these composites, ONERA developed a model called pseudo-tensorial which allows to take into account several orientations of cracks but remains easy to implement and to interpret contrary to tensorial model. The scalar and pseudo-tensorial models differ only by the cracks families taken into account (see figure 1). For the scalar model, three damage variables associated with the principal axes of the material are defined. In the pseudo-tensorial model two additional damage variables are considered respectively in the directions +45° and -45° with respect to the orthotropy directions. The pseudo-tensorial model allows to take into account the loss of orthotropy in out-of-axis tests.

COMPARISON WITH EXPERIMENTS

The general characteristics of the experimental and calculated traction compression curves show good agreement for both in-axes and out-of-axes tests (CAST3M calculations were performed in this case on a single 8 nods cubic element). In the case of 45° (angle between the tensile direction and the first fibre direction) traction compression test, the pseudo-tensorial model that allows 2 additional cracking directions compared to the scalar one reproduces better the out-of-axes behaviour (see figure 2.1 and 2.2). During recompression, while the scalar model shows a decrease of the Young modulus (not observed experimentally), the pseudo-tensorial model reproduces better the experimental curves.

COMPARISON CAST3M AND ZeBuLoN IN THE CASE OF A NOTCHED PLATE

In order to verify the good implementation of the models in CAST3M, results obtained in the case of a notched plate submitted to traction in the direction (0/90°) with respect to the fibres directions were compared with ZeBuLoN results. Despite to the fact they do not correspond to the same view point, it can be seen from figures 3 and 4 that the damage calculated from the two codes agree as well as for their localisation and their intensity. The damage d_1 corresponding to cracks planes perpendicular to the fibre direction named 1 (see figure 1 for damage variables definition) is displayed in figure 3. It develops mainly perpendicular to the tensile direction. Figures 4.1 and 4.2 indicate that the damages corresponding to cracks plane perpendicular to the direction at 45° and – 45° from the first fibre direction, this is to say d_{+45} and d_{-45} develop mainly respectively orientated at -45° and 45° with respect to the tensile direction. There is no damage in the plane perpendicular to the second fibre direction (itself perpendicular to the tensile direction) so that variable d_2 is identically equal to zero.

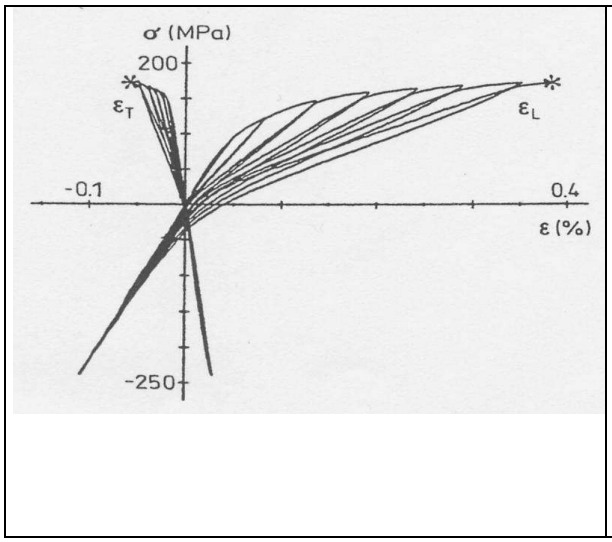

Figure 2.1: 45° tension/compression test Experimental results on a woven SiC_f/SiC [1]. ε_L: longitudinal strain, ε_T: transversal strain.

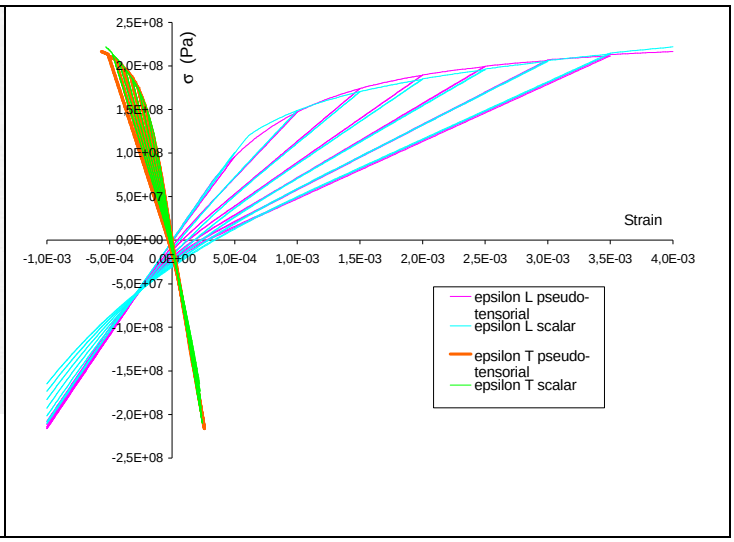

Figure 2.2: 45° traction-compression test. Pseudo-tensorial and scalar model results. Longitudinal strain, ε_L, transversal strain, ε_T.

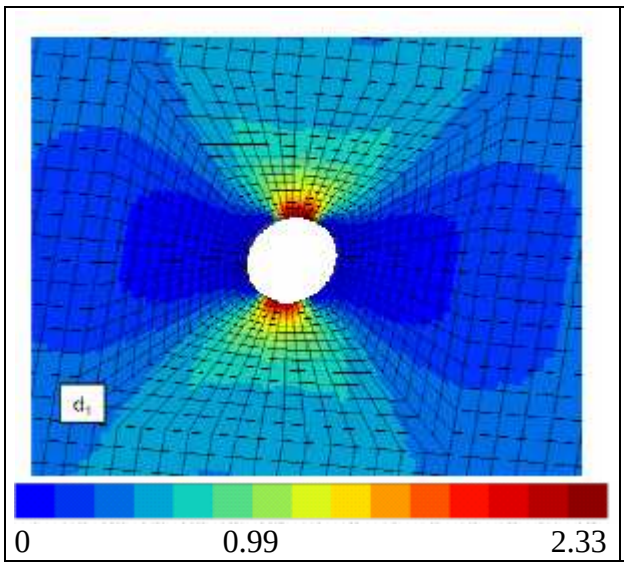

Figure 3.1:Damage variable d1 , ZeBuLoN

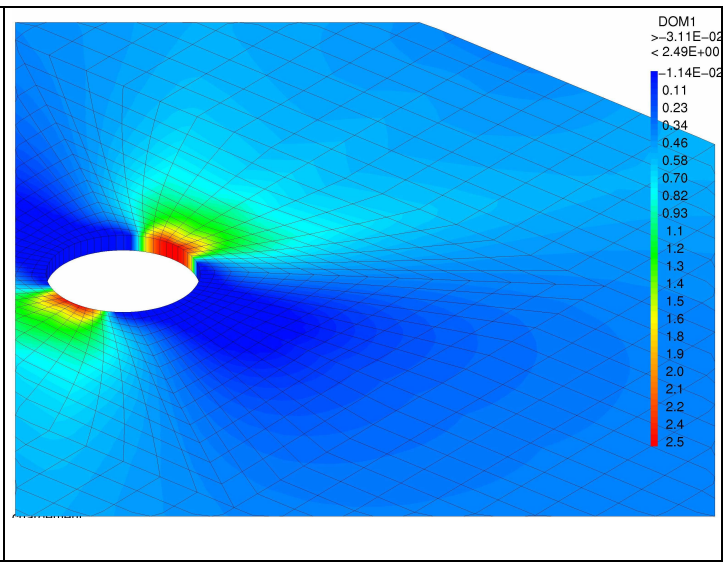

Figure 3.2: Damage variable d1, CAST3M

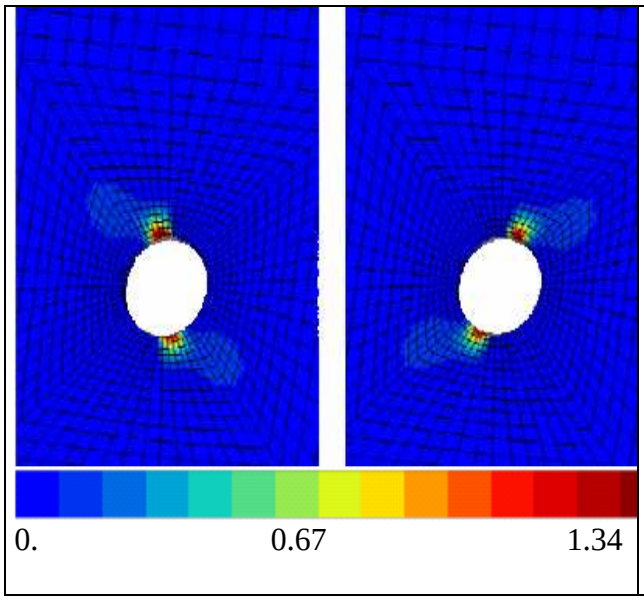

Figure 4.1: Damage variables d_{+45} (left) and d_{-45} (right), ZeBuLoN.

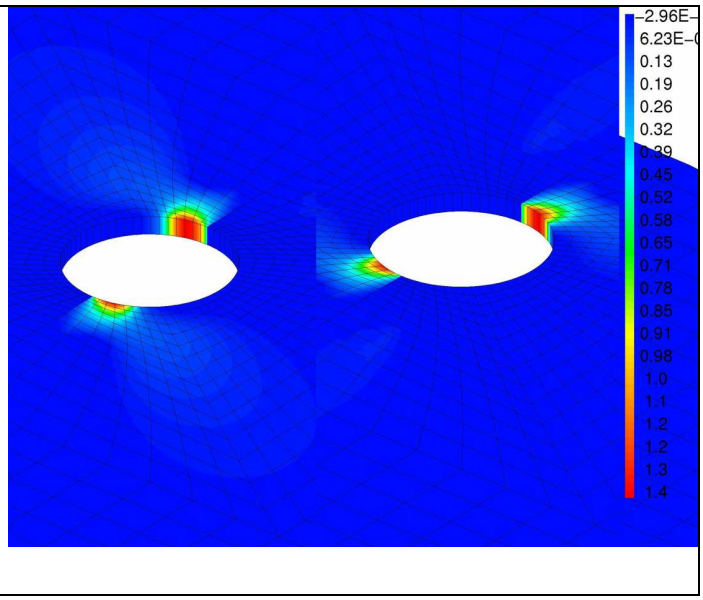

Figure 4.2: Damage variables d_{+45} (left) and d_{-45} (right), CAST3M.

CONCLUSIONS

The new models for SiC_f/SiC thermo-mechanical modelling were successfully implemented in CAST3M. They were used to model a divertor using the same mesh and loading as those described in the previous work of A. Li puma et al. [2]. The results reported in [8] indicate, as for elastic calculations and those performed with the previously developed model [3], that the Tauro criteria is exceeded on the inner wall (inner surface) but with a less important extent. Due to the additional damage directions taken into account, damage distribution is more physical using the pseudo-tensorial model. The new laws could also be used in the future to model the lower scales of SiC_f/SiC such as plies, fibres or matrix. The materials parameters in the lower scales could be identified by the inverse method. In the next years, implementation in CAST3M of multiscale modelling adapted to SiC_f/SiC will be continued.

REFERENCES

[1] P. Ladevèze, A. Grasser and O. Allix, Journal of Engineering Materials and Technology, 116 (1994) 331-336.

[2] A. Li Puma, L. Giancarli, Y. Poitevin, J. Szczepanski, Rapport DM2S/SERMA/LCA/RT/02-3189/A.

[3] G. Aiello, Utilisation des composites à matrice céramique SiC_f/SiC comme matériau de structure de composant interne du tore d'un réacteur à fusion, Thèse de Doctorat, Université d'Evry Val d'Essonne, Thesis (2001), EVRY0002.

REPORTS AND PUBLICATIONS

[4] C. Guerin, 'Multi-scale modelling for SiC_f /SiC composites, Preliminary considerations to an implementation in CAST3M'. DM2S/SEMT/LM2S/RT/04-001/A, january 2004.

[5] J. F. Maire and N. Carrère, 'Modélisation multi-échelles des composites SiC_f /SiC. Définition des potentiels thermodynamiques et de dissipation pour les différents constituants du composites SiC_f /SiC. ONERA Report RT 1/09795/DMSE – mars 2005.

[6] N. Carrère and J. F. Maire, 'Modélisation multi-échelles des composites SiC_f /SiC. Fourniture des éléments nécessaires à l'implémentation d'une méthode de changement d'échelle pour les passages micro-méso et méso-macro adaptée au SiC_f /SiC' ONERA Report RT 2/09795/DMSE – mars 2005.

[7] C. Rospars, N. Carrere, J. F. Maire and C. Guerin, 'Multi-scale modelling of the thermo-mechanical behaviour of SiC_f /SiC advanced composite. Definition of the constitutive laws and gathering of the data necessary for the implementation in CAST3M'. DM2S/SEMT/LM2S/RT/05-016/A.

[8] N. Carrère, J. F. Maire and F. Laurin , 'Modélisation multi-échelles des composites SiC_f /SiC. Fourniture des éléments nécessaires à l'implémentation d'une méthode de changement d'échelle pour les passages micro-méso et méso-macro adaptée au SiC_f /SiC' ONERA Report RT 2/09795/DMSE – décembre 2005.

[9] N. Carrère, J. F. Maire, F. Laurin, O. Fandeur and C. Guerin, 'Implementation in CAST3M of new models developed at ONERA for SiC_f/SiC composite. Comparison of CAST3M and Zebulon Results. Tests and application to the case of a divertor'. Report DM2S/SEMT/RT/05-034.

TASK LEADER

Caroline GUERIN

DEN/DM2S/SEMT/LM2S
CEA-Saclay
F-91191 Gif-sur-Yvette Cedex

Tel. : 33 1 69 08 53 52
Fax : 33 1 69 08 86 84

e-mail : cguerin@cea.fr